Monthly Notices
of the
ROYAL ASTRONOMICAL SOCIETY

MNRAS **459,** 771–778 (2016)
Advance Access publication 2016 March 28

doi:10.1093/mnras/stw695

Keck/MOSFIRE spectroscopy of five ULX counterparts

M. Heida,[1,2,3]★ P. G. Jonker,[2,3] M. A. P. Torres,[2,4] T. P. Roberts,[5] D. J. Walton,[1,6] D.-S. Moon,[7] D. Stern[6] and F. A. Harrison[1]

[1]*Space Radiation Laboratory, California Institute of Technology, Pasadena, CA 91125, USA*
[2]*SRON Netherlands Institute for Space Research, Sorbonnelaan 2, NL-3584 CA Utrecht, the Netherlands*
[3]*Department of Astrophysics/IMAPP, Radboud University Nijmegen, PO Box 9010, NL-6500 GL Nijmegen, the Netherlands*
[4]*European Southern Observatory, Alonso de Cordova 3107, Casilla 19001, Vitacura, Santiago 19, Chile*
[5]*Department of Physics, University of Durham, South Road, Durham DH1 3LE, UK*
[6]*Jet Propulsion Laboratory, California Institute of Technology, 4800 Oak Grove Drive, Pasadena, CA 91109, USA*
[7]*Department of Astronomy and Astrophysics, University of Toronto, Toronto, ON M5S 3H4, Canada*

Accepted 2016 March 22. Received 2016 February 25; in original form 2015 November 5

ABSTRACT

We present *H*-band spectra of the candidate counterparts of five ultraluminous X-ray sources (ULXs; two in NGC 925, two in NGC 4136 and Holmberg II X-1) obtained with Keck/MOSFIRE (Multi-Object Spectrometer for Infra-Red Exploration). The candidate counterparts of two ULXs (J022721+333500 in NGC 925 and J120922+295559 in NGC 4136) have spectra consistent with (M-type) red supergiants (RSGs). We obtained two epochs of spectroscopy of the candidate counterpart to J022721+333500, separated by 10 months, but discovered no radial velocity variations with a 2σ upper limit of 40 km s^{-1}. If the RSG is the donor star of the ULX, the most likely options are that either the system is seen at low inclination ($<40^{\circ}$) or the black hole mass is less than 100 M$_{\odot}$, unless the orbital period is longer than 6 years, in which case the obtained limit is not constraining. The spectrum of the counterpart to J120922+295559 shows emission lines on top of its stellar spectrum, and the remaining three counterparts do not show absorption lines that can be associated with the atmosphere of a star; their spectra are instead dominated by emission lines. Those counterparts with RSG spectra may be used in the future to search for radial velocity variations, and, if those are present, determine dynamical constraints on the mass of the accretor.

Key words: infrared: stars – X-rays: individual: Holmberg II X-1 – X-rays: individual: [SST2011] J022721.52+333500.7 – X-rays: individual: [SST2011] J022727.53+333443.0 – X-rays: individual: CXOU J120922.6+295551 – X-rays: individual: [SST2011] J120922.18+295559.7.

1 INTRODUCTION

Ultraluminous X-ray sources (ULXs) are point-like, off-nuclear X-ray sources with a luminosity in the 0.3–10 keV band $>10^{39}$ erg s^{-1} (see Feng & Soria 2011 for a review). This is higher than the Eddington luminosity of a 10 M$_{\odot}$ black hole (BH), which raises the question how ULXs attain their high luminosities. The majority of (candidate) ULXs, with $L_{\rm X}<10^{41}$ erg s^{-1}, likely contain stellar mass BHs ($M_{\rm BH} \leq 20$ M$_{\odot}$) accreting at or above their Eddington limit (Middleton et al. 2015 and references therein), although some of these ULXs could still contain massive stellar ($M_{\rm BH} = 20$–100 M$_{\odot}$) or even intermediate-mass BHs ($M_{\rm BH} = 100$–10^5 M$_{\odot}$; Colbert & Mushotzky 1999). The most luminous ULXs, with $L_{\rm X}>10^{41}$ erg s^{-1} (referred to as hyperluminous X-ray sources), are hard to explain as stellar mass BHs, and are strong candidates to host BHs more massive than those found in X-ray binaries in our Galaxy (Strohmayer & Mushotzky 2003; Farrell et al. 2009; Casares & Jonker 2014; Pasham, Strohmayer & Mushotzky 2014).

To date, there are only two ULXs with mass estimates that do not depend on modelling of their X-ray spectra (Liu et al. 2013; Motch et al. 2014). In both cases, although the uncertainties on the masses are large, a stellar mass BH is favoured as the accretor. In addition, Bachetti et al. (2014) discovered X-ray pulsations from M82 X-2, proving that the accretor in that ULX is a neutron star.

Improved model-independent mass measurements of ULX accretors are necessary to prove that the so-called 'ultraluminous state' (Gladstone, Roberts & Done 2009) is indeed a sign of super-Eddington accretion on to stellar mass BHs, to see if neutron star accretors are common among ULXs, and to find out if some ULXs contain massive stellar or intermediate-mass BHs. Dynamical mass measurements would be the most reliable method. Through

★ E-mail: mheida@caltech.edu

phase-resolved spectroscopic observations, it may be possible to trace the radial velocity curve of the donor and measure the mass function, setting a lower limit on the mass of the compact object. In the optical regime, attempts to measure the mass function in this way have been hampered by the presence of bright accretion discs in these systems (Roberts et al. 2011; Liu, Orosz & Bregman 2012). However, some ULXs may have red supergiant (RSG) donor stars, and these can outshine the disc in the near-infrared (NIR) part of the spectrum (Copperwheat et al. 2005).

In Heida et al. (2014), we describe our systematic search for NIR counterparts to nearby ULXs. We discovered 11 candidate counterparts that could be RSG donor stars. NIR spectroscopy with the Very Large Telescope has shown that one of these candidate counterparts, to RX J004722.4−252051 in NGC 253, is indeed an M-type RSG, with a peculiar velocity suggestive of a massive stellar BH accretor (Heida et al. 2015). In this paper, we describe the results of our observations with the Keck telescope that yielded NIR spectra of five other ULX counterparts from the Heida et al. (2014) sample. Two of the ULXs are situated in NGC 925 and two in NGC 4136. The fifth ULX is Holmberg II X-1 (hereafter Ho II X-1). Three of these ULXs (J022721+333500 in NGC 925 and J120922+295551 and J120922+295559 in NGC 4136) have been observed to reach maximum X-ray luminosities of a few times 10^{39} erg s^{-1}; J022727+333443 in NGC 925 and Ho II X-1 are brighter, reaching X-ray luminosities of a few times 10^{40} erg s^{-1} (Liu & Bregman 2005; Grisé et al. 2010; Swartz et al. 2011). The goal of this campaign was to characterize the NIR counterparts. Hence, we initially obtained only one epoch of data per source. Based on these observations, we obtained a second epoch for one source in NGC 925, J022721+333500, to search for radial velocity shifts.

This paper is organized as follows: in Section 2 we describe the setup of our observations. Section 3 describes our data reduction and analysis. In Section 4, we present the results for the separate counterparts and in Section 5 we discuss our findings and conclude.

2 OBSERVATIONS

We obtained *H*-band spectra of five ULX counterparts with the Multi-Object Spectrometer for Infra-Red Exploration (MOSFIRE; McLean et al. 2010, 2012), mounted on the Keck I telescope on Mauna Kea.[1] MOSFIRE has a field of view of 6.1 arcmin × 6.1 arcmin with a pixel scale of 0.18 arcsec and a robotic slit mask system with up to 46 slits. The data were taken on 2013 December 22, 2014 January 10 (programme ID C241M) and 2014 November 4 (programme ID C201M; all dates are in UT). We used slit masks with 0.7-arcsec-wide slits which give us, in combination with the *H*-band filter and the fixed MOSFIRE diffraction grating, a spectral resolution $R \approx 3000$ and spectral coverage from ∼14 500 to 18 000 Å. The seeing on all nights was >0.7 arcsec (∼0.8–1.0 arcsec), so that the resolution is set by the slit width. The integration time per exposure was 119.3 s on all nights. On 2013 December 22 and 2014 January 10, we used an ABBA nodding pattern with a nod amplitude of 1.5 arcsec along the slit. On 2014 November 4, we used a different slit orientation than we did for the observations of NGC 925 in 2013 December and 2014 January (see also Fig. 1). The orientation used in the first observations was chosen to avoid other nearby objects – the new orientation was chosen to better separate the two components of the elongated counterpart of J022721+333500;

[1] The data will be publicly available 18 months after the observations in the Keck Observatory Archive (https://koa.ipac.caltech.edu).

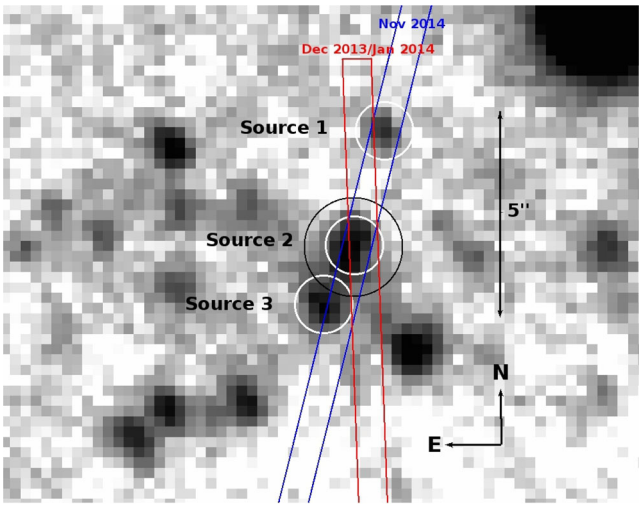

Figure 1. WHT/LIRIS *H*-band image of J022721+333500 in NGC 925, with the MOSFIRE slit positions indicated by red (2013 December /2014 January observations) and blue (2014 November observations) boxes. The black circle indicates the *Chandra* X-ray localization of the ULX. The white circles indicate the sources visible in our 2014 November MOSFIRE observation. Source 3 is not centred on the slit, causing an offset ≤85 ± 10 km s^{-1} in its measured radial velocity.

however, the seeing was not good enough to distinguish the two components. As a result, there were multiple sources in the slit containing J022721+333500, so we used an ABBA nodding pattern with a larger nod amplitude (2.9 arcsec for the first 20 exposures and 3.4 arcsec for the remaining 71 exposures). The total exposure times are listed in Table 1. We observed telluric standard stars at similar airmass as the science targets before and after every series of exposures. No flux standards were observed. For every slit mask configuration, we obtained flats and arc spectra in the afternoon before the observing run.

3 DATA REDUCTION AND ANALYSIS

We reduce the data with the MOSFIRE Data Reduction Pipeline version 2014.03.14 (MOSFIRE-DRP; described in detail by Steidel et al. 2014). The pipeline handles the background subtraction and combines the separate exposures to produce a 2D, rectified and wavelength-calibrated spectrum for every slit. The wavelength calibration is done by fitting a polynomial to the night sky lines, using wavelengths in vacuum. The typical standard deviation of the residuals after fitting is 0.1 Å (∼2 km s^{-1} at 1.65 μm). For every observing night and target, we split the science exposures into two groups of at most 1.5 h and reduce them separately.

We then use the STARLINK program FIGARO to extract the spectra with the *profile* and *optextract* tasks (Horne 1986). In the 2014 November observation of J022721+333500, we extract spectra of three objects that are visible in the slit. To correct for telluric absorption, we use the IDL routine XTELLCOR_GENERAL (Vacca, Cushing & Rayner 2003).

For the final analysis (characterization of the spectra and – if possible – cross-correlation with template spectra to measure radial velocities), we use Tom Marsh's program MOLLY. We load the wavelength-calibrated spectra into MOLLY and first run the task *hfix* to calculate the heliocentric velocity. Because the spectra are not flux calibrated, we normalize them by fitting a third-order polynomial and dividing by it. This removes any systematic flux offsets,

Table 1. Description of the Keck/MOSFIRE observations. Apparent and absolute *H*-band magnitudes from Heida et al. (2014) are also provided. The last column describes the features that are visible in the NIR spectrum.

Host galaxy	Source	H	M_H	Observation date (UT)	Time on source (h)	Spectral features
NGC 925	J022721+333500	18.7	−10.6	2013 Dec. 22 and 2014 Jan. 10	5.4	RSG
	(Source 2)			2014 Nov. 4	3	
NGC 925	J022727+333443	20.1	−9.2	2013 Dec. 22 and 2014 Jan. 10	5.4	Em. lines
NGC 4136	J120922+295551	19.1	−10.8	2014 Jan. 10	2.4	Em. lines
NGC 4136	J120922+295559	19.2	−10.7	2014 Jan. 10	2.4	RSG + em. lines
Holmberg II	Ho II X-1	20.6	−7.1	2014 Jan. 10	2.6	Em. lines

which is important to do before we average the spectra of every target. The only exception is J022727+333443, since it has no continuum that can be used for the normalization. Next, we rebin them to a common velocity scale of 30.25 km s^{-1} pixel^{-1} using *vbin*, which also moves the spectra to the heliocentric frame. Finally, we average the spectra of every target per night. As expected, because the orbital periods for ULXs with an RSG donor are ≥3 years, we do not observe velocity shifts between the spectra taken in 2013 December and 2014 January, and therefore we add them to increase the signal-to-noise ratio (S/N).

For J022721+333500 and J120922+295559, we use *xcor* to cross-correlate the spectra with template spectra of a range of spectral types (that have been normalized in the same way as our science spectra). As templates we use model RSG spectra from Lançon et al. (2007), with solar abundances, a mass of 15 $M_\odot$ and temperatures ranging from 2900 to 5000 K. In the spectra of J022721+333500 and J120922+295559, we mask the regions with high noise levels due to strong telluric emission lines. With *xcor* we apply shifts to the spectrum of −10 to +30 pixels, with steps of 1 pixel, and calculate the value of the cross-correlation function for each pixel shift. *xcor* then computes the radial velocity difference between spectrum and template by fitting a parabola to the cross-correlation function at the peak pixel and its two neighbouring pixels. We follow Heida et al. (2015) to obtain a more robust measure of the uncertainty on the radial velocity measurements: we use the MOLLY command *boot* to produce 1000 bootstrapped copies of the spectra, and use *xcor* to cross-correlate them with one of the model spectra (with $T_{\rm eff}$ = 3500 K). The resulting distribution of radial velocities is Gaussian. We fit a Gaussian curve to this distribution and adopt the centroid and width of this Gaussian as a robust estimate of the radial velocity and its uncertainty. To check for signs of rotational broadening of the absorption lines in the RSG spectra, we broaden a template spectrum (with $T_{\rm eff}$ = 3500 K) with 10–200 km s^{-1} in steps of 10 km s^{-1}. We then cross-correlate those broadened template spectra with the RSG spectra to see if the cross-correlation improves for higher rotational velocities.

For the spectra where we detect emission lines, we use the MOLLY command *mgfit* to fit Gaussian profiles to the positions of [Fe II] and/or hydrogen Brackett lines in the spectra, and calculate their offset with respect to their rest wavelengths.

4 RESULTS

4.1 NGC 925: J022721+333500

In the NIR image of NGC 925 (see Fig. 1), the counterpart to J022721+333500 appears elongated. Due to the orientation of the slits that we used for the observations in 2013 December and 2014 January, only one object (source 2 in Fig. 1) is visible in those observations. In the 2014 November observations, we used a slit orientation to better separate the components of the counterpart, but the seeing was not good enough to resolve them. In these observations, spectra of three objects are visible. Source 2 (see Fig. 1) corresponds to the elongated counterpart. All three spectra (sources 1 to 3) show a continuum with many absorption lines from neutral metals. The CO bandheads at 1.62 and 1.66 μm are also detected, proving that the objects are all K- or M-type stars (see Fig. 2 for the spectrum of source 2). We find no evidence for velocity broadening of the absorption lines. This is fully consistent with what we expect for RSGs, which have rotational velocities of at most a few km s^{-1}, undetectable at MOSFIRE's resolution of ∼80 km s^{-1} in the *H* band.

From the cross-correlation with template spectra, we find a radial velocity of 495 ± 11 km s^{-1} for source 1. For source 2, we find a radial velocity of 506 ± 9 km s^{-1} for the Dec. 2013/Jan. 2014 spectrum and 500 ± 14 km s^{-1} for the Nov 2014 spectrum. For source 3, we find a radial velocity of 502 ± 8 km s^{-1}. This source is not centred on the slit, which causes an offset in the radial velocity. The sources are too faint to be visible in our through-slit alignment images. However, brighter stars selected to check the slit alignment were detected and we use the comparison of their locations on the through-slit image with that of the deep WHT/LIRIS image (Heida et al. 2014) to determine the actual location of the slit on the sky. From this, we derive a best estimate of the offset between the location of source 3 and the centre of the slit of 0.5 arcsec ± 0.05 arcsec (see Fig. 1). This corresponds to 2.8 ± 0.3 pixels on the MOSFIRE detector, or a velocity offset of 85 ± 10 km s^{-1}. Because the seeing was comparable to the slit width, this value is an upper limit on the velocity offset. If we correct for this, we find a radial velocity ≥420 ± 15 km s^{-1} for source 3. The radial velocities of sources 1 and 2 are in agreement with what is expected from the radial velocity field of NGC 925 (de Blok et al. 2008). This proves that the objects are located in NGC 925, confirming the absolute magnitude reported for source 2 in Heida et al. (2014). That absolute magnitude is such that even if source 2 consists of two equally bright sources, they are both RSGs. The radial velocity of source 3 is somewhat offset with respect to the local radial velocity, but that source is still most likely located in NGC 925. The highest values for the cross-correlation function for all sources are found when cross-correlating with the templates with the lowest temperatures, indicating that these NIR sources are probably M-type stars.

4.2 NGC 925: J022727+333443

The counterpart to J022727+333443 shows no continuum emission at all. The spectrum is dominated by a single strong emission line due to [Fe II] with a rest wavelength of 1.644 μm. Many weaker emission lines are visible, due to [Fe II], H (Brackett lines), He I, He II and H_2. These are indicated in Fig. 3. We fitted Gaussian profiles to these emission lines to calculate the radial velocity of the

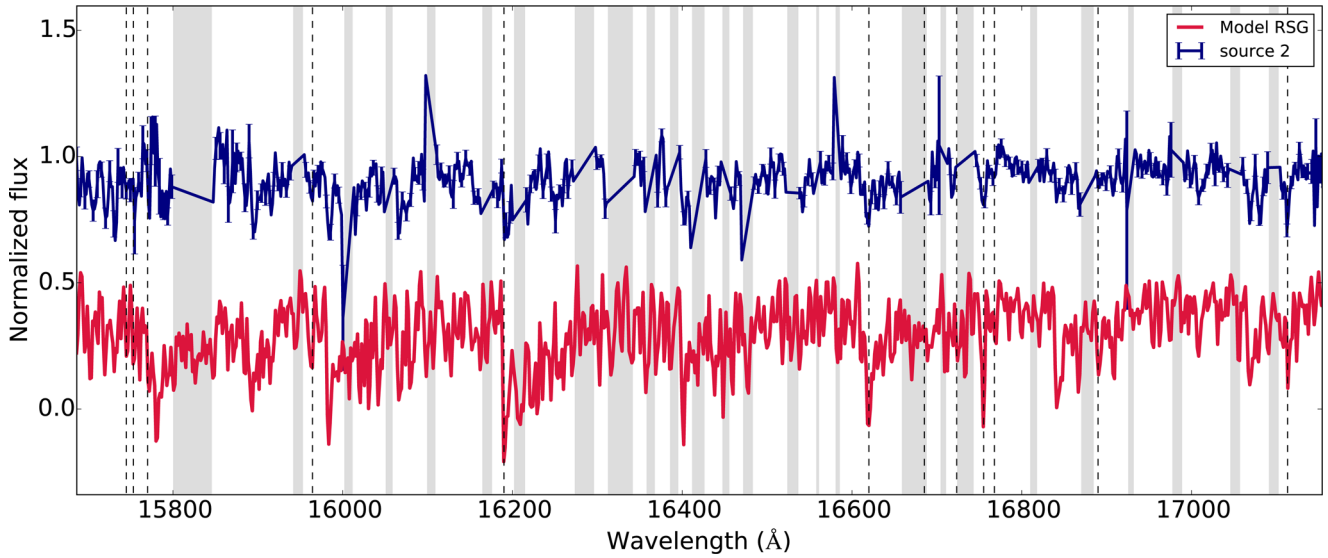

Figure 2. The normalized spectra of NGC 925 J022721+333500 (source 2, from the Dec. 2013/Jan. 2014 observation, blue line) and a 3500 K model from Lançon et al. (2007, red line, shifted downwards by 0.5 for clarity). The spectrum of J022721+333500 has been shifted by −506 km s^{-1} and has been interpolated over wavelength ranges that were strongly affected by noise from telluric emission lines (grey shaded areas). The 'emission lines' visible near some of these ranges are due to this noise. The dashed lines indicate the positions of absorption lines that are indicative of late-type stars – from short to long wavelength: Mg I triplet (1.574, 1.575, 1.577 μm), Si I (1.59 μm), CO bandhead (1.62 μm), CO bandhead (1.66 μm), Si I (1.67 μm), Al I triplet (1.672, 1.675, 1.676 μm), OH (1.69 μm) and Mg I (1.71 μm).

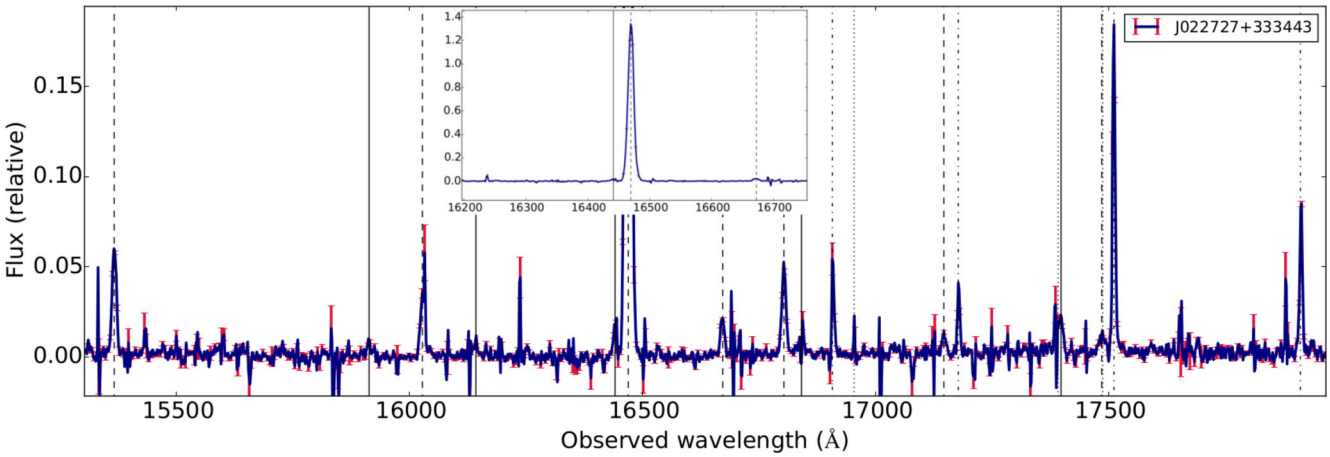

Figure 3. The MOSFIRE spectrum of NGC 925 J022727+333443. Error bars (in red) are plotted for every third data point. Dotted lines indicate positions of He lines, dashed lines indicate positions of [Fe II] lines, solid lines indicate the H Brackett series and dot–dashed lines indicate positions of H_2 lines. The vertical lines representing spectral transitions are redshifted by 540 km s^{-1}. The inset shows the full profile of the [Fe II]λ1.644 emission line.

counterpart. The [Fe II], hydrogen and helium lines are well fitted by a Gaussian, but the H_2 lines are asymmetric. The radial velocity of the lines is 540 ± 2 km s^{-1}, proving that the source is part of NGC 925 and not a foreground or background object.

4.3 Ho II X-1

Ho II X-1 is a well-studied nearby ULX. It is surrounded by a nebula powered by the X-ray source that was discovered in optical observations (e.g. Pakull & Mirioni 2002; Lehmann et al. 2005). Our NIR spectrum shows a weak continuum with emission lines, most notably the [Fe II] (λ1.644) line and the hydrogen Brackett lines (see Fig. 4). We do not significantly detect any absorption lines. The S/N in the continuum is ∼4, which is too low to detect absorption lines from an RSG if they would be present. From the positions of the emission lines, we calculate a radial velocity of 165 ± 3 km s^{-1}, consistent with the radial velocity of the galaxy and earlier observations of the nebula.

4.4 NGC 4136: J120922+295551

The spectrum of the counterpart of J120922+295551 resembles that of Ho II X-1, with a weak continuum and emission lines (see Fig. 5). The 2D spectrum shows spatially extended emission around the position of the ULX, with stronger Brackett emission lines further from the ULX. The radial velocity of the counterpart as measured from the shift of the [Fe II] line is 550 ± 5 km s^{-1}, proving that the source is located in NGC 4136. The continuum emission could be due to an RSG. The S/N in the continuum is ∼5, and the strongest absorption line in an RSG, the CO bandhead at 1.62 μm, lies in a

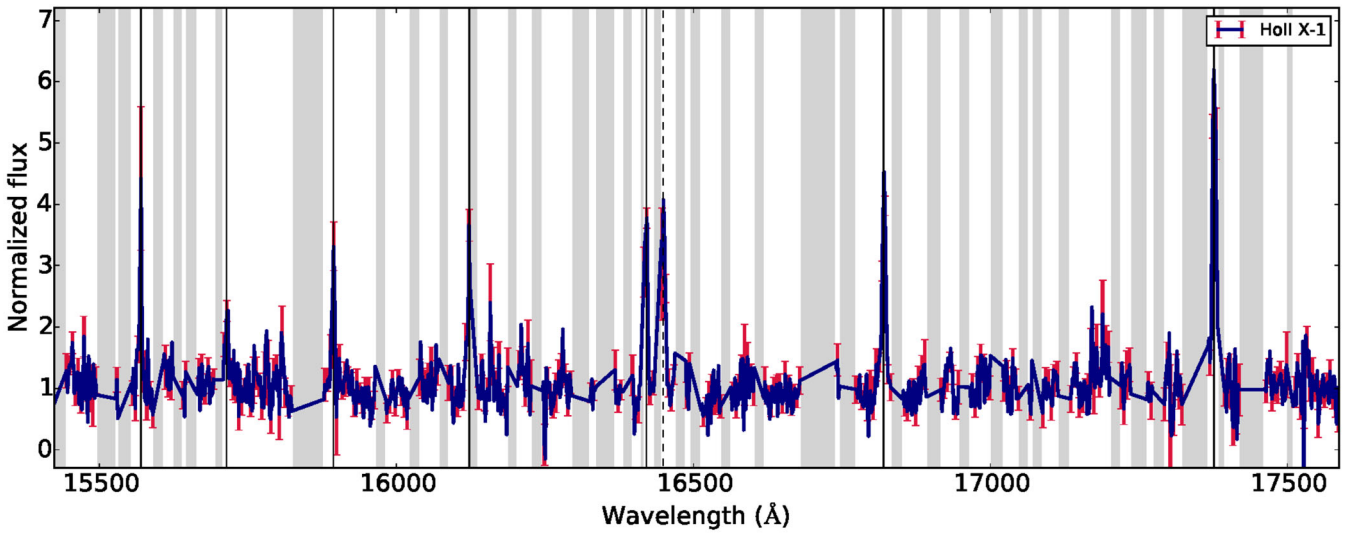

Figure 4. The normalized MOSFIRE spectrum of Ho II X-1. The spectrum has been interpolated over wavelength ranges that were strongly affected by noise from telluric emission lines (grey shaded areas). Error bars (in red) are plotted for every third data point. The dashed line indicates the [Fe II] (λ1.644) line and the solid lines indicate the positions of the hydrogen Brackett lines. The vertical lines representing spectral transitions are redshifted by 165 km s^{-1}.

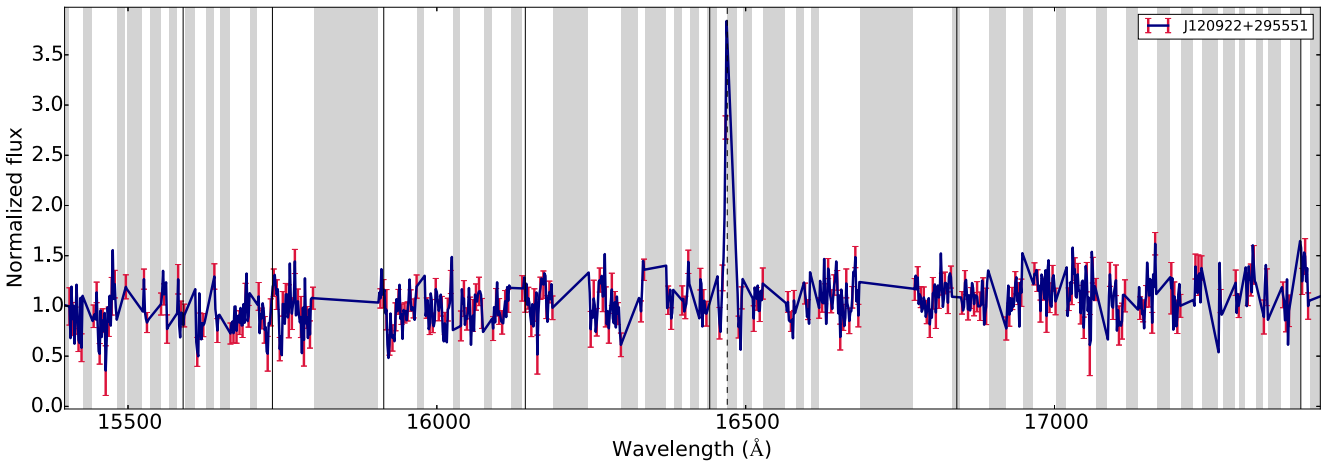

Figure 5. Part of the normalized MOSFIRE spectrum of NGC 4136 J120922+295551. The spectrum has been interpolated over wavelength ranges that were strongly affected by noise from telluric emission lines (grey shaded areas). Error bars (in red) are plotted for every third data point. The dashed line indicates the [Fe II] (λ1.644) line and the solid lines indicate the positions of the hydrogen Brackett lines. The vertical lines representing spectral transitions are redshifted by 550 km s^{-1}.

region that is heavily affected by noise from telluric emission lines, precluding us from detecting this feature. Other RSG absorption lines would not be significant at this S/N.

4.5 NGC 4136: J120922+295559

The spectrum of J120922+295559 shows continuum emission with absorption lines due to neutral metals and CO, indicative of late-type stars (see Fig. 6). However, the strongest feature in the spectrum is the [Fe II] (λ1.644) emission line (dash–dotted line), similar to J022727+333443 and J120922+295551. Weaker emission lines are visible at the positions of the hydrogen Brackett lines that are in regions uncontaminated by noise from telluric emission lines, most notably at the position of the Br (10–4) line at 1.74 μm. Visual inspection of the 2D spectrum reveals that the peak of the [Fe II] emission is spatially offset by ∼0.8 arcsec with respect to the continuum emission, corresponding to a distance of ∼45 pc. The Br (10–4) line does not show this spatial offset.

In late-type stars, the CO bandhead at 1.62 μm is the strongest absorption feature. Unfortunately, in the J120922+295559 spectrum, this bandhead is redshifted into a region heavily contaminated by noise from telluric emission lines, precluding us from reliably detecting it. There is an absorption feature visible at the position of the CO bandhead at 1.66 μm, as well as at the positions of the Si I line at 1.59 μm, the Al I triplet (1.672, 1.675, 1.676 μm), the OH line at 1.69 μm and the Mg I line at 1.71 μm. The cross-correlation with model RSGs yields a radial velocity of 586 ± 22 km s^{-1}, consistent with the radial velocity of NGC 4136 at the location of the ULX (Fridman et al. 2005) and thus proving that the source is indeed located in that galaxy. The highest values for the cross-correlation function are achieved with the templates with temperatures of 2900–4000 K, pointing towards an M-type RSG. We find no evidence for rotational broadening of the absorption lines.

We measure the radial velocity offset of the emission lines by fitting Gaussian profiles to the [Fe II] (λ1.644) and Br (10–4) lines while masking the parts of the spectrum that contain absorption

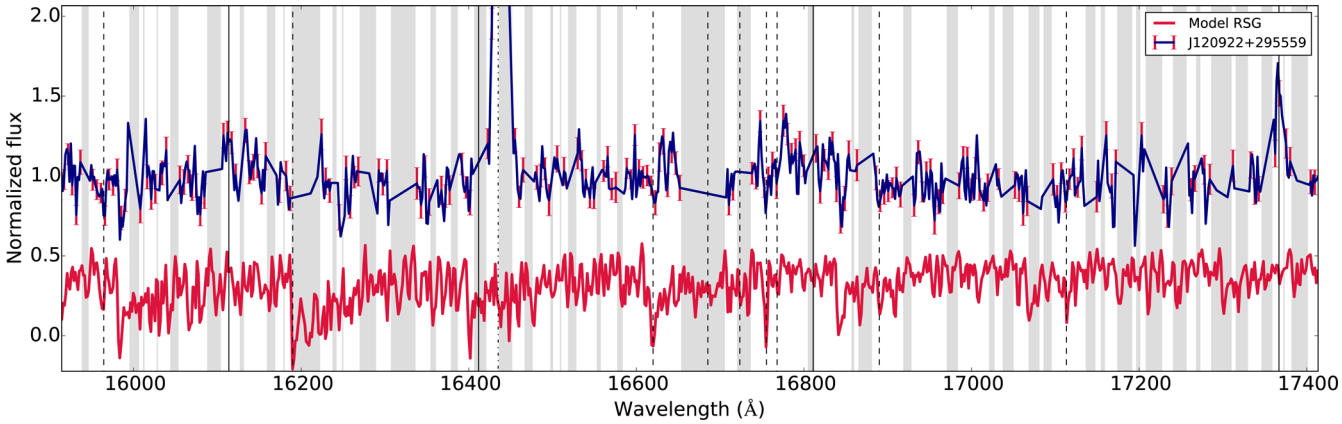

Figure 6. The normalized spectra of NGC 4136 J120922+295559 (blue line, with error bars – in red – plotted at every third data point), and a 3500 K model from Lançon et al. (2007, red line, shifted downwards by 0.5 for clarity). The spectrum of J120922+295559 has been shifted by −586 km s^{-1} and has been interpolated over wavelength ranges that were strongly affected by noise from telluric emission lines (grey shaded areas). Solid lines indicate the positions of hydrogen Brackett lines and dashed lines indicate the positions of absorption lines that are indicative of late-type stars – from short to long wavelength: Si I (1.59 μm), CO bandhead (1.62 μm), CO bandhead (1.66 μm), Si I (1.67 μm), Al I triplet (1.672, 1.675, 1.676 μm), OH (1.69 μm) and Mg I (1.71 μm). The dash–dotted line indicates the position of the [Fe II] (1.644 μm) emission line, the peak of which lies at 4.7 (relative units).

lines. Fitting the two lines separately, we find that their radial velocities are consistent with being the same within the error bars. Fitting them simultaneously to reduce the uncertainty, we find a radial velocity of 570 ± 4 km s^{-1}, consistent with the velocity of the RSG.

5 DISCUSSION AND CONCLUSIONS

We obtained Keck/MOSFIRE *H*-band spectra of five ULX counterparts, two located in NGC 925, two in NGC 4136 and Ho II X-1. Two of these, J022721+333500 in NGC 925 and J120922+295559 in NGC 4136, are consistent with being M-type supergiants. The absorption lines in such spectra can in principle be used to measure the radial velocity curve of the counterpart and obtain a lower limit on the BH mass.

5.1 Emission line spectra

The emission lines in the spectra of J022727+333443, Ho II X-1, J120922+295551 and J120922+295559 can have several origins. They may originate in a nebula, or in the accretion disc – although the latter is ruled out for the [Fe II] line in J120922+295559, as it is spatially offset from the spectrum of the counterpart. None of the sources we observed show double-peaked emission lines, which argues against an accretion disc origin for these lines, unless we view the disc under a low inclination angle. These emission lines cannot be used for dynamical mass measurements. However, like nebular emission lines observed in optical spectra of some ULXs (cf. Pakull & Mirioni 2002; Kaaret, Ward & Zezas 2004; Moon et al. 2011), they may be used to infer the true X-ray luminosity of ULXs, and help in determining whether or not the X-ray emission of these sources is beamed. The observed line intensity ratio in NGC 925 J022727+333443 of [Fe II] (1.644) to Br-10 is ∼71.5. If we use 0.330 as the ratio of Br-10 to Brγ line intensities for case B gas in the temperature range of 5000–20 000 K (Draine 2011), we have ∼24 as the ratio of the [Fe II] intensity to Brγ. This is somewhat lower than what has been observed in several Galactic supernova remnants where the ratio has been estimated to be ≥27 and up to 80 (and possibly higher; see Koo et al. 2007 and references therein). Given the relatively low ionization potential, 7.9 eV, of Fe, this indicates that the ionization source of the [Fe II] and H I lines in NGC 925 may be harder than the typical shocks found in Galactic supernova remnants. Strong [Fe II], H I recombination and H_2 lines have all been detected in the mid-infrared spectra of the highly obscured high-mass X-ray binary IGR J16318−4848 (Moon et al. 2007). The lines are believed to be originating in X-ray illuminated dense circumstellar material from the strong mass-loss of the optical companion star potentially evolving into an luminous blue variable (LBV). The similarity supports the interpretation that there is ample material around the ULX. We will discuss the origin and implications of these emission lines in more detail in a forthcoming paper.

The apparent and absolute magnitudes mentioned in Table 1 are those of the combined flux in the emission lines and the continuum emission. To estimate the magnitude of a possible donor star, we estimate the magnitude of the continuum. Because we did not observe a flux standard star to calibrate our spectra, we do this by comparing the S/N level for the continuum emission to values calculated with the MOSFIRE exposure time calculator[2] for our observing conditions and a range of magnitudes. We find that for Ho II X-1, the flux in the emission lines does not contribute significantly to the magnitude of the counterpart. For J022727+333443 in NGC 925, we find a limit on the apparent magnitude of $H \gtrsim 22.5$, corresponding to an absolute magnitude $M_H \gtrsim -7$. This makes it unlikely that the donor star is a supergiant of spectral type F or later (Tokunaga 2000). For J120922+295551 in NGC 4136, we find an apparent magnitude of $H \approx 20.5$, corresponding to an absolute magnitude $M_H \approx -9.4$. If the continuum emission in this source is mainly due to the donor star, this absolute magnitude would mean it is still most likely an RSG. A deeper observation might then reveal stellar absorption lines.

5.2 RSG spectra

The RSG candidate counterpart of the ULX RX J004722.4−252051 in NGC 253 (Heida et al. 2015) shows a radial velocity that is offset with respect to its environment by 66 ± 6 km s^{-1}. The candidate donor stars of J022721+333500 and J120922+295559

[2] http://www2.keck.hawaii.edu/inst/mosfire/etc.html

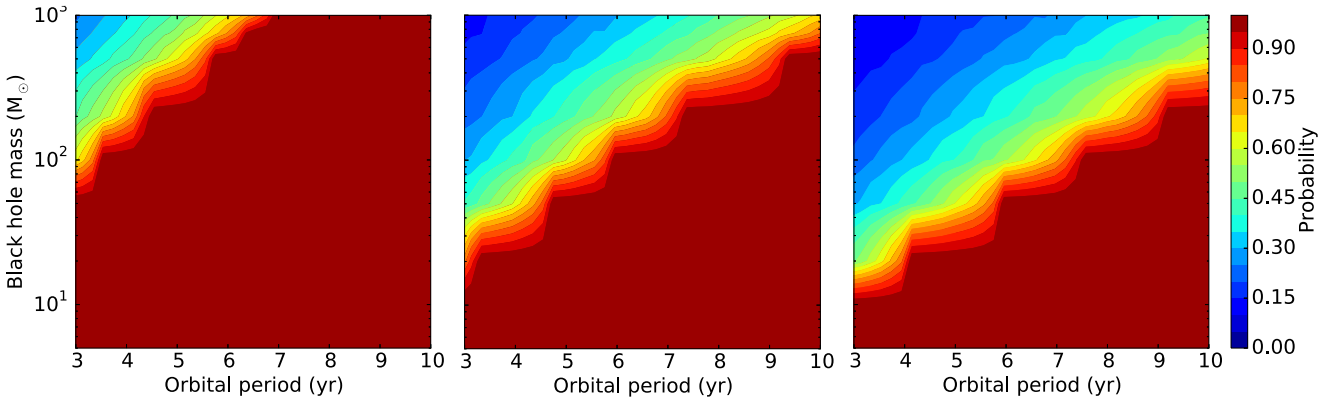

Figure 7. The probability that the radial velocities measured in our two spectra of NGC 925 J022721+333500 obtained 10 months apart are consistent within 40 km s^{-1}, as a function of BH mass and orbital period, for system inclinations of 20°, 40° and 60° (left to right). We assume a mass of 10 M$_\odot$ for the RSG and that mass transfer happens through Roche lobe overflow. Orbital periods shorter than 3 years are ruled out given the radius of an M-type RSG. The step-like shape is due to the discrete sampling of BH masses.

do not show such an offset, although source 3 in our *H*-band image of the environment of J022721+333500 may show a velocity offset, with an upper limit of 80 km s^{-1}, with respect to sources 1 and 2. Analogous to RX J004722.4−252051 in NGC 253, this offset could be due to binary motion of the RSG around a massive stellar BH or to a natal kick imparted on the BH in the supernova explosion, if source 3 would be the donor star of the ULX. However, this seems unlikely based on the 95 per cent confidence error circle of the X-ray position of the ULX in Fig. 1. Alternatively, source 3 may be a runaway RSG (e.g. Eldridge, Langer & Tout 2011).

Among these three candidate donor stars, J120922+295559 in NGC 4136 is the only one that also shows emission lines in its NIR spectrum, strengthening its association with the ULX. Optical emission lines from an H II region close to the ULX are visible in the spectrum of RX J004722.4−252051 in NGC 253, but no emission lines were detected in the NIR part of its spectrum. The counterpart to J022721+333500 in NGC 925 also does not show NIR emission lines. Following the same procedure as in Heida et al. (2015), we calculate the probability that this NIR source is an interloper that happens to coincide with the ULX. We compute the density of NIR sources that are as bright as or brighter than the ULX candidate counterpart in our WHT/LIRIS *H*-band image (see Heida et al. 2014 for details). We only consider the bottom 1/3 of the image, because NGC 925 occupies that part of the detector. In this area of 2×10^4 arcsec^2, we detect 99 sources. The 95 per cent confidence error circle of the position of the X-ray source on the *H*-band image has an area of 4.1 arcsec^2. Thus, the probability of a chance superposition is approximately 2 per cent. Based on this, we cannot exclude that the NIR source is an interloper, although the probability is rather low.

The counterpart of J022721+333500 is elongated in our *H*-band image, but during our Keck/MOSFIRE observations, seeing conditions were not good enough to allow us to separate the spectra of the two putative components. The peak-to-peak distance of the elongated core in our LIRIS image is ∼0.7 arcsec. An adaptive optics-assisted or *Hubble Space Telescope* NIR image at ∼0.1 arcsec resolution would be useful to confirm whether or not the counterpart in our LIRIS image consists of two individual sources. If this is the case, a bore-sight corrected *Chandra* position of the ULX, with a localization error of ∼0.2 arcsec, could distinguish whether one of these is the counterpart of the ULX or if the NIR source and ULX are unrelated.

The ultimate proof that the RSG is orbiting a BH can only come from the detection of periodic shifts of its radial velocity. We obtained two epochs of spectroscopy of the candidate counterpart and found no change in the radial velocity, with a 2σ upper limit of 40 km s^{-1}. Assuming that the RSG is the donor star in a binary system, the probability that we would not detect a velocity shift between two measurements depends on the orbital period, ratio of the mass of the donor star to the mass of the BH and the inclination of the system. We calculate this probability by drawing 10 000 random values for the orbital phase at the time of the first observation, and calculating how many of these result in a velocity shift smaller than our observed upper limit for a range of BH masses, orbital periods and system inclinations. Here we assume that mass transfer happens through Roche lobe overflow, as wind-feeding is unlikely to be a viable mechanism for ULXs (Copperwheat et al. 2007). The results of this calculation are shown in Fig. 7 for system inclinations of 20°, 40° and 60°. The upper limit of 40 km s^{-1}, with the measurements taken 308 d apart, puts very weak restraints on the orbital period or BH mass if the system inclination is <40°. For $i = 40°$, BH masses larger than ∼100 M$_\odot$ in combination with orbital periods shorter than ∼4 years would likely (probability >50 per cent) have led to a velocity difference larger than 40 km s^{-1} and would thus have been detected. For $i \geq 60°$, the same BH masses in combination with orbital periods shorter than ∼6 years would likely have led to a detection. Given the expected radius of an M-type RSG, orbital periods shorter than 3 years can be ruled out as the Roche radius would then be too small to contain the RSG. If the RSG is the donor star of the ULX, the most likely options are that either the system is seen at low inclination or the BH mass is less than 100 M$_\odot$, unless the orbital period is longer than 6 years.

The stellar absorption lines in the spectra of J022721+333500 and J120922+295559 make them excellent targets for dynamical mass measurements of BHs in ULXs, if these RSGs are indeed the donor stars of the ULXs. However, as the non-detection of a radial velocity shift in J022721+333500 shows, we will need observations over time spans of many years to cover the expected orbital periods of these systems: first to confirm or rule out that these RSGs show radial velocity variations, and if they do, to measure their full radial velocity curve and set a lower limit to the mass of the BH.

ACKNOWLEDGEMENTS

MH would like to thank Nick Konidaris for his help with the MOSFIRE DRP. We thank Tom Marsh for developing MOLLY. TPR acknowledges support from STFC as part of the consolidated grant award ST/L00075X/1. The work of DJW and DS was carried out at

Jet Propulsion Laboratory, California Institute of Technology, under a contract with NASA. PGJ acknowledges support from ERC consolidator grant number 647208. The data presented herein were obtained at the W. M. Keck Observatory, which is operated as a scientific partnership among the California Institute of Technology, the University of California and the National Aeronautics and Space Administration. The Observatory was made possible by the generous financial support of the W. M. Keck Foundation. We wish to recognize and acknowledge the very significant cultural role and reverence that the summit of Mauna Kea has always had within the indigenous Hawaiian community. We are most fortunate to have the opportunity to conduct observations from this mountain.

REFERENCES

Bachetti M. et al., 2014, Nature, 514, 202
Casares J., Jonker P. G., 2014, Space Sci. Rev., 183, 223
Colbert E. J. M., Mushotzky R. F., 1999, ApJ, 519, 89
Copperwheat C., Cropper M., Soria R., Wu K., 2005, MNRAS, 362, 79
Copperwheat C., Cropper M., Soria R., Wu K., 2007, MNRAS, 376, 1407
de Blok W. J. G., Walter F., Brinks E., Trachternach C., Oh S.-H., Kennicutt R. C., Jr, 2008, AJ, 136, 2648
Draine B. T., 2011, Physics of the Interstellar and Intergalactic Medium. Princeton Univ. Press, Princeton, NJ
Eldridge J. J., Langer N., Tout C. A., 2011, MNRAS, 414, 3501
Farrell S. A., Webb N. A., Barret D., Godet O., Rodrigues J. M., 2009, Nature, 460, 73
Feng H., Soria R., 2011, New Astron. Rev., 55, 166
Fridman A. M., Afanasiev V. L., Dodonov S. N., Khoruzhii O. V., Moiseev A. V., Sil'chenko O. K., Zasov A. V., 2005, A&A, 430, 67
Gladstone J. C., Roberts T. P., Done C., 2009, MNRAS, 397, 1836
Grisé F., Kaaret P., Feng H., Kajava J. J. E., Farrell S. A., 2010, ApJ, 724, L148
Heida M. et al., 2014, MNRAS, 442, 1054
Heida M. et al., 2015, MNRAS, 453, 3510
Horne K., 1986, PASP, 98, 609
Kaaret P., Ward M. J., Zezas A., 2004, MNRAS, 351, L83
Koo B.-C., Moon D.-S., Lee H.-G., Lee J.-J., Matthews K., 2007, ApJ, 657, 308
Lançon A., Hauschildt P. H., Ladjal D., Mouhcine M., 2007, A&A, 468, 205
Lehmann I. et al., 2005, A&A, 431, 847
Liu J., Orosz J., Bregman J. N., 2012, ApJ, 745, 89
Liu J.-F., Bregman J. N., 2005, ApJS, 157, 59
Liu J.-F., Bregman J. N., Bai Y., Justham S., Crowther P., 2013, Nature, 503, 500
McLean I. S. et al., 2010, Proc. SPIE, 7735, 77351E
McLean I. S. et al., 2012, Proc. SPIE, 8446, 84460J
Middleton M. J., Heil L., Pintore F., Walton D. J., Roberts T. P., 2015, MNRAS, 447, 3243
Moon D.-S., Kaplan D. L., Reach W. T., Harrison F. A., Lee J.-E., Martin P. G., 2007, ApJ, 671, L53
Moon D.-S., Harrison F. A., Cenko S. B., Shariff J. A., 2011, ApJ, 731, L32
Motch C., Pakull M. W., Soria R., Grisé F., Pietrzyński G., 2014, Nature, 514, 198
Pakull M. W., Mirioni L., 2002, preprint (arXiv:astro-ph/0202488)
Pasham D. R., Strohmayer T. E., Mushotzky R. F., 2014, Nature, 513, 74
Roberts T. P., Gladstone J. C., Goulding A. D., Swinbank A. M., Ward M. J., Goad M. R., Levan A. J., 2011, Astron. Nachr., 332, 398
Steidel C. C. et al., 2014, ApJ, 795, 165
Strohmayer T. E., Mushotzky R. F., 2003, ApJ, 586, L61
Swartz D. A., Soria R., Tennant A. F., Yukita M., 2011, ApJ, 741, 49
Tokunaga A. T., 2000, Allen's Astrophysical Quantities, 4th edn. Am. Inst. Phys., New York, p. 143
Vacca W. D., Cushing M. C., Rayner J. T., 2003, PASP, 115, 389

This paper has been typeset from a TEX/LATEX file prepared by the author.